Broadband epsilon-near-zero metamaterials with steplike metal-dielectric multilayer structures

Lei Sun, Jie Gao, and Xiaodong Yang*

Department of Mechanical and Aerospace Engineering, Missouri University of Science and Technology, Rolla, Missouri 65409, USA

(Received 31 July 2012; revised manuscript received 16 April 2013; published 26 April 2013)

The concept of the broadband epsilon-near-zero meta-atom consisting of layered stacks with specified metallic filling ratio and thickness is proposed based on the Bergman spectral representation of the effective permittivity. The steplike metal-dielectric multilayer structures are designed to achieve realistic broadband epsilon-near-zero meta-atoms in optical frequency range. These meta-atoms can be integrated as building blocks for unconventional optical components with exotic electromagnetic properties over a wide frequency range, such as the demonstrated broadband directional emission and phase front shaping.

DOI: 10.1103/PhysRevB.87.165134 PACS number(s): 42.25.Bs, 78.20.Ci, 78.67.Pt, 81.05.Zx

I. INTRODUCTION

Metamaterials are artificially structured materials with subwavelength components, which can be designed to create extraordinary macroscopic electromagnetic properties that do not exist in nature.[1–11] Among all kind of metamaterials, the metamaterials with near-zero permittivity [epsilon-near-zero (ENZ)] emerge into the focus of the extensive exploration due to their anomalous electromagnetic features at microwave and optical frequencies.[12–23] However, all ENZ metamaterials suffer from single frequency response for the near-zero permittivity, which gives a huge disadvantage for practical applications.

In this paper, we further develop the theoretical strategy[24] for mathematically designing the broadband ENZ metamaterials based on the Bergman spectral representation[25,26] of the effective permittivity, and propose the realistic broadband ENZ meta-atoms by applying the steplike metal-dielectric multilayer structures. In quasistatic conditions, the Bergman spectral representation expresses the effective permittivity of a composite medium in terms of a series of residue-singularity couples. Therefore, the broadband ENZ metamaterial can be flexibly designed in a dimensionless spectral space, while the geometric information of the metamaterial, including the dimensions and the filling ratio of each component, can be obtained through a proper inverse problem. According to this strategy, the steplike metal-dielectric multilayer structures are proposed to realize the broadband ENZ meta-atoms in optical frequency range. Functional optical devices constructed by the realistic broadband ENZ meta-atoms are also demonstrated, and exotic electromagnetic properties of such devices are explored including the broadband directional emission and phase front shaping.

II. DESIGN OF BROADBAND ENZ META-ATOM

As depicted in Fig. 1(a), the proposed broadband ENZ meta-atom is a two-dimensional three-layer stack with the dimensions of 100×25 nm. Each layer of the meta-atom is a metal-dielectric mixture with gold (Au) as the metallic inclusion and silica (SiO_2) as the dielectric host medium. The permittivity of gold follows the simple Drude model $\varepsilon_{\mathrm{Au}} = \varepsilon_\infty - \omega_p^2/(\omega(\omega + i\gamma))$ with dielectric constant $\varepsilon_\infty = 5.7$, plasma frequency $\omega_p = 1.3666 \times 10^{16}$ rad/s, and damping constant $\gamma = 3 \times 4.0715 \times 10^{13}$ rad/s. Here the damping constant is of the value three times higher than the bulk value in order to account for surface scattering, grain boundary effects, and inhomogeneous broadening of the metal thin film. The permittivity of silica is $\varepsilon_{\mathrm{SiO_2}} = 2.1338$. In quasistatic conditions, the Bergman spectral representation expresses the effective permittivity of the meta-atom as

$$\varepsilon_e = \varepsilon_{\mathrm{SiO_2}}(1 - F(s)), \tag{1}$$

with respect to the variable $s = \varepsilon_{\mathrm{SiO_2}}/(\varepsilon_{\mathrm{SiO_2}} - \varepsilon_{\mathrm{Au}})$. The spectral function $F(s)$ reads

$$F(s) = \sum_{i=1}^{3} \frac{F_i}{s - s_i}, \tag{2}$$

which is analytic everywhere with positive residue F_i except for three simple singularities s_i confined as $0 \leqslant s_1 < s_2 < s_3 < 1$. Correspondingly, based on the geometric structure of the stack, including the filling ratio f_i of the gold inclusion in each layer and the thickness d_i of each layer, the effective permittivity ε_x of the whole stack reads

$$\varepsilon_x(s) = \varepsilon_{\mathrm{SiO_2}} \left[\sum_{i=1}^{3} \frac{d_i/d}{1 - f_i/s} \right]^{-1}, \tag{3}$$

with the total stack thickness $d = \sum_{i=1}^{3} d_i$. Through the effective permittivity, the connection between the singularities and residues in the spectral space [Eq. (1)] and the geometric structure of the stack in the physical space [Eq. (3)] can be set up as

$$\varepsilon_{\mathrm{SiO_2}} \left[1 - \sum_{i=1}^{3} \frac{F_i}{s - s_i} \right] = \varepsilon_{\mathrm{SiO_2}} \left[\sum_{i=1}^{3} \frac{d_i/d}{1 - f_i/s} \right]^{-1}. \tag{4}$$

Clearly, the variable s is only a function of the frequency ω as $s = s(\omega)$, which implies the Bergman spectral representation on the left-hand side of Eq. (4) describes the effective permittivity of the stack only as a function of the frequency ω. Therefore, for designing the broadband ENZ meta-atom, it is simple to request that

$$\mathrm{Re}(\varepsilon_x(s(\omega_j))) = \varepsilon_{\mathrm{SiO_2}} \mathrm{Re} \left[1 - \sum_{i=1}^{3} \frac{F_i}{s(\omega_j) - s_i} \right] = 0, \tag{5}$$

with respect to a series of specified frequencies ω_j ($j = 1,2,3$) in a wide frequency range $[\omega_a, \omega_b]$. Regarding the

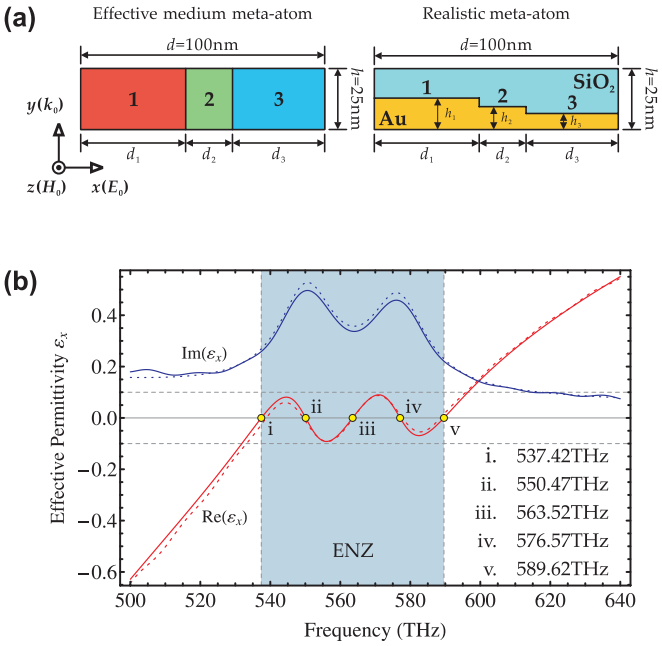

FIG. 1. (Color online) The schematic diagram of the broadband ENZ meta-atom and the designed broadband near-zero effective permittivity. (a) The effective-medium meta-atom with three homogenous layers composed by gold and silica, and the realistic meta-atom with a steplike metal-dielectric multilayer structure. (b) The theoretical values (solid curves) and the FDTD retrieved values (dashed curves) of the real part (red curves) and the imaginary part (blue curves) of the effective permittivity ε_x of the effective medium meta-atom, with the ENZ frequencies (yellow dots) listed at the right bottom.

mathematical structure of Eqs. (3) and (5), the value of the singularity s_i in Eq. (5) can be set as $s_1 = 0$ and $s_i = \mathrm{Re}(s(\omega_i))$ for $i = 2,3$ with respect to another series of specified frequencies ω_i within $[\omega_a, \omega_b]$. The specified frequency ω_i and ω_j can be simply arranged as an equally spaced array based on the following confinement:

$$\omega_a = \omega_{j=1} < \omega_{i=2} < \omega_{j=2} < \omega_{i=3} < \omega_{j=3} = \omega_b. \quad (6)$$

Therefore, the residue F_i can be fully determined by Eq. (5). With the value of the residue F_i and the singularity s_i, the filling ratio f_i and the thickness d_i of the broadband ENZ meta-atom can be achieved from Eq. (4). It is worth noting that this strategy is suitable for designing multilayered meta-atom for realizing other constant permittivity over a wide frequency range in principle, and the number of stack layers is not limited. In order to confine the optical loss within a moderate range, the operating frequency range of the broadband ENZ meta-atom in Fig. 1(a) is set between $\omega_a = 537.42$ THz and $\omega_b = 589.62$ THz, and the filling ratio f_i of the gold inclusion and the thickness d_i of each layer are designed and listed in Table I. According to the results, the realistic meta-atom, shown in the right panel of Fig. 1(a), is also designed as a three-layer stack with the same thickness d_i of each layer, but each layer is replaced by a gold-silica multilayer structure, where the height h_i of the gold is $h_i = f_i h$ $(i = 1,2,3)$ with respect to the same filling ratio f_i of the gold inclusion. It is worth mentioning that in practical fabrication, the feature size

TABLE I. Filling ratio of the gold inclusion and the thickness of each layer.

Layer	f_i	d_i (nm)
1	0.216329	43.6884
2	0.188523	19.2691
3	0.163955	37.0425

of the fabricated thin film has the accuracy of a nanometer, and a detailed analysis on the robustness of the designed parameters is presented in the Appendix.

The effective permittivity ε_x of the effective medium meta-atom is plotted in Fig. 1(b) with the red curves standing for the real part and blue curves standing for the imaginary part (the optical loss). Moreover, the solid curves indicate the theoretical value of ε_x based on Eq. (5), while the dashed curves indicate the retrieved value, which is calculated from the scattering parameters (S_{11} and S_{21}) of the effective medium meta-atom from the full-wave finite-difference time-domain (FDTD) method. Five equally spaced frequencies (ENZ frequency), at which the value of ε_x equals to zero, are listed at the right bottom of the figure and marked as yellow dots on the curve. ENZ frequencies i, iii, and v represent the frequency ω_j, while ii and iv stand for the frequency ω_i. It is clear that the FDTD retrieved results match the theoretical results well, with only small fluctuations caused by the inevitable phase variation of the reflected electromagnetic wave from different stack layers in the effective medium meta-atom, which is not included in the theoretical strategy. Additionally, the value of the effective permittivity ε_y of the effective medium meta-atom is $\varepsilon_y \approx 2.8 + 0.001i$ in the operating frequency range.

The upper panel of Fig. 2 gives the distributions of the absolute value of the electric field inside the effective medium meta-atom with a height of 250 nm at the five ENZ frequencies with the electromagnetic wave directly

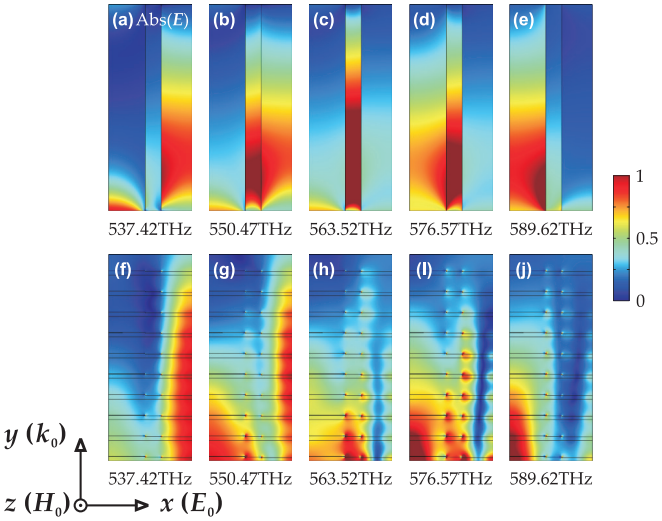

FIG. 2. (Color online) The distributions of the absolute value of the electric field in the effective medium meta-atom (upper panel) and the realistic meta-atom array (lower panel) at different ENZ frequencies, corresponding to the incident electromagnetic wave indicated by the coordinates.

illuminating from the bottom of the meta-atom, while the lower panel of Fig. 2 shows the electric field inside the realistic meta-atom array with the same height (including 10 realistic meta-atoms along the y direction). As indicated in Fig. 2, the electric field is strongly confined and guided through the meta-atom along different paths with respect to different ENZ frequencies, due to the continuity of the electric displacement with near-zero permittivity. The properly designed filling ratio of the gold inclusion in each stack layer ensures the zero effective permittivity around each specified ENZ frequency. Then the corresponding thickness of each stack layer modifies the interactions between the adjacent layers, resulting in the broadband ENZ response across the desired frequency range. Additionally, the similar distribution of the electric field inside the effective medium meta-atom and the realistic meta-atom array, although disturbed by the inevitable scattering caused by the realistic structures, informs that the realistic meta-atom also possesses a similar broadband ENZ response that is coincident with the theoretical design.

III. ANALYSIS OF BROADBAND ENZ OPTICAL DEVICES

Functional optical devices with broadband response corresponding to the broadband ENZ property can be constructed by the realistic broadband ENZ meta-atom. For example, Fig. 3(a) schematically gives a prism made of the meta-atoms in air, with an oblique upper surface of angle θ for realizing the directional emission of electromagnetic waves. The incoming electromagnetic wave with vertical wave vector $\boldsymbol{k}_{\text{in}}$ and Poynting vector $\boldsymbol{S}_{\text{in}}$ can be collimated inside the prism as it crosses the lower interface from air, while the refracted outgoing electromagnetic wave with the wave vector $\boldsymbol{k}_{\text{out}}$ and Poynting vector $\boldsymbol{S}_{\text{out}}$ will be normal to the upper interface. Physically, the directional emission is resulted in the conservation of the tangential component of the wave vectors at the upper interface between the prism and air, which can be explained by the flat elliptical iso-frequency contour (IFC) of the meta-atom compared with the circular IFC of air with radius $k_0 = 2\pi/\lambda$ in Figs. 3(b) and 3(c). Clearly, the propagating direction of the outgoing electromagnetic wave will be quite close to the normal direction (k_y' direction) of the upper interface of the prism without the consideration of material loss [Fig. 3(b)], but slightly bend away when the material loss is taken into account [Fig. 3(c)].

Correspondingly, Fig. 4 gives the simulation results of the directional emission for prisms made of effective medium [Fig. 4(a)] and realistic meta-atoms [Fig. 4(b)] with an oblique interface of $\theta = 15^\circ$ at the designed ENZ frequency of 537.42 THz. The distribution of the electric

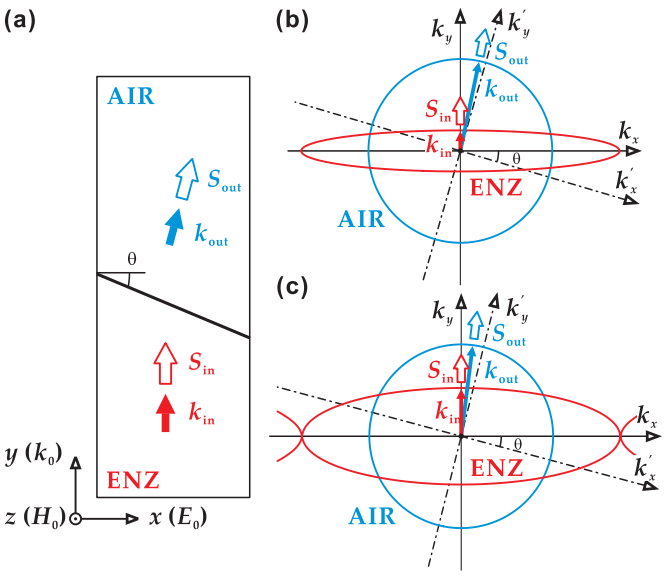

FIG. 3. (Color online) The schematic diagram and IFC analysis about the directional emission with respect to the broadband ENZ response. (a) The diagram of the directional emission through the ENZ prism represented by the electromagnetic waves inside and outside the prism. (b) The flat elliptical IFC (red curve for $\varepsilon_x = 0.05$ and $\varepsilon_y = 3.0$) of the meta-atom under lossless condition. (c) The elliptical-like IFC (red curve for $\varepsilon_x = 0.05 + 0.5i$ and $\varepsilon_y = 3.0 + 0.002i$) of the meta-atom under lossy condition. The IFC of air is plotted as blue circle.

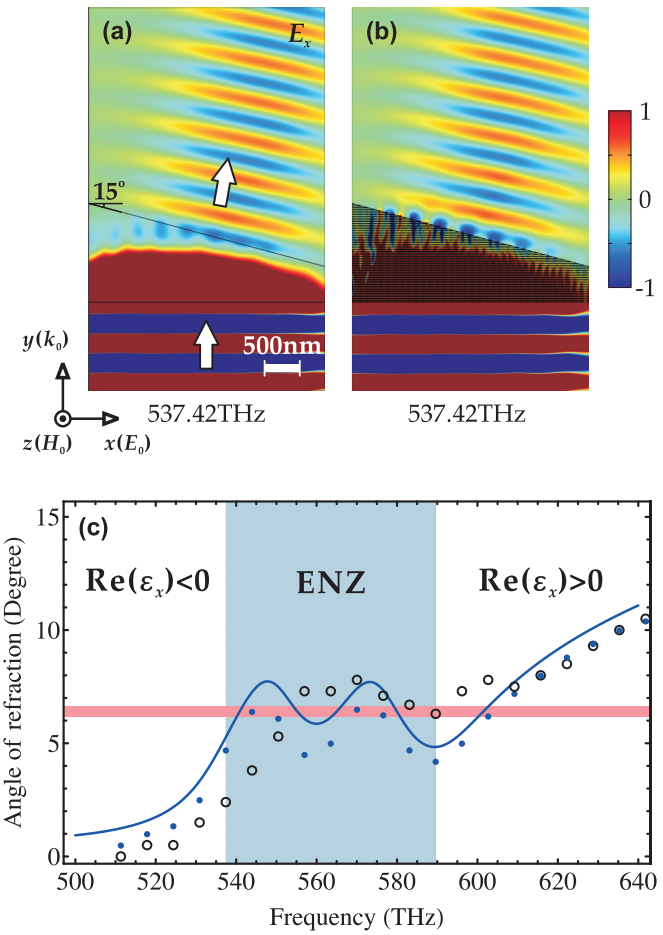

FIG. 4. (Color online) Simulation results about the directional emission of the broadband ENZ prism with the 15°-oblique upper interface, represented by the distribution of the electric field amplitude E_x and the power flow (hollowed arrows), for (a) the effective medium made prism and (b) the realistic meta-atom made prism. (c) The angle of refraction (in degrees) as a function of the frequency, based on the theoretical effective permittivity (blue curve), and the simulation results of the effective medium made prism (blue dots) and the realistic meta-atom made prism (black circles). The average angle of refraction is 6.3° (red line) in the ENZ frequency range.

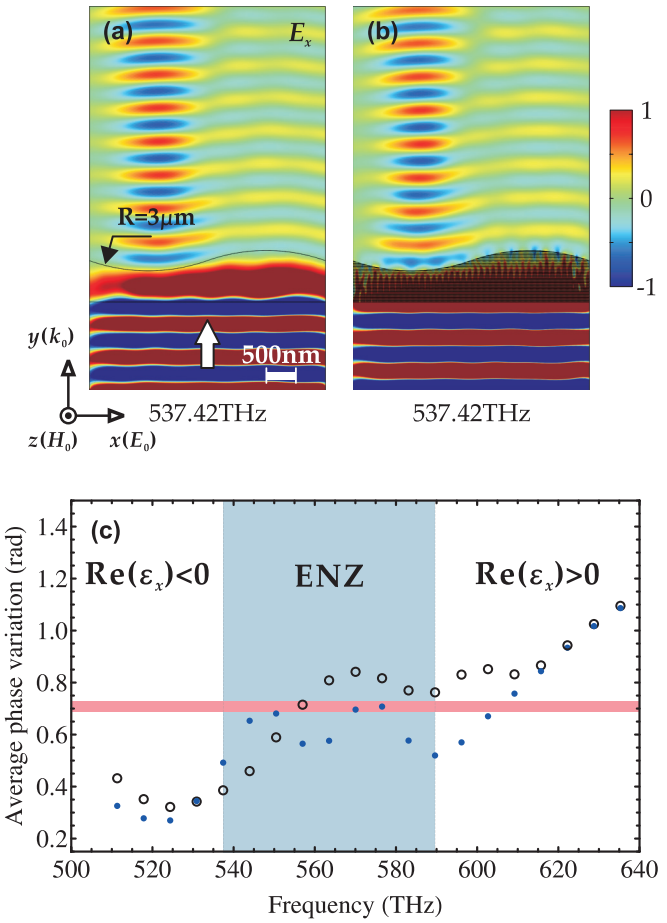

FIG. 5. (Color online) Simulation results about the phase front shaping of the broadband ENZ S-shape lens with the radius of curvature of 3 μm, represented by the distribution of the electric field amplitude E_x, for (a) the effective medium made S-shape lens and (b) the realistic meta-atom made S-shape lens. (c) The average phase variation (in radians) as a function of the frequency, with respect to the effective medium made S-shape lens (blue dots) and the realistic meta-atom made S-shape lens (black circles). The mean value of the average phase variation is 0.7 rad (red line) in the ENZ frequency range.

field amplitude E_x is displayed, with the power flow indicated by hollowed arrows. Strong reflection occurs at the bottom of the prism due to the mismatched impedance (analysis about the impedance matching to free space is given in the Appendix), while the near-zero phase variation of the propagating electromagnetic wave inside the prism and the small angle of refraction of the outgoing electromagnetic wave at the upper interface of the prism are observed due to the near-zero permittivity. Furthermore, the variation of the angle of refraction with respect to different frequencies [Fig. 4(c)] reveals the broadband ENZ response of the realistic meta-atom made prism, through the comparison among the theoretical results obtained from the Snell's law (blue curve), the simulation results of the effective medium prism (blue dots), and the simulation results of the realistic meta-atom made prism (black circles). It is worth mentioning that the deviations of the simulation results of the realistic meta-atom made prism is due to the inevitable material loss and scatterings caused by the internal structures, and the average angle of refraction of the realistic meta-atom made prism is about 6.3° (red line) in the designed operating frequency range, representing an effective group index of $n_g = 0.42$.

Because of the relatively small phase variation caused by the near-zero permittivity, the realistic broadband ENZ meta-atom can also be used to build optical devices for shaping the phase front of electromagnetic waves as the S-shape lens example shown in Fig. 5. The example is demonstrated at the ENZ frequency of 537.42 THz for S-shape lenses made of effective medium [Fig. 5(a)] and realistic meta-atoms [Fig. 5(b)], with the results indicated by the distribution of the electric field amplitude E_x. Clearly, the uniform phase pattern of the electromagnetic wave inside the S-shape lens due to the near-zero permittivity leads to a phase front of the outgoing electromagnetic wave conformal to the upper interface of the S-shape lens, although not exactly matches surface geometry especially for the realistic meta-atom made S-shape lens, because of the inevitable scattering caused by the structure. Besides, it is worth noting that the electric field amplitude is not uniformly distributed in the space above the lens, because the electromagnetic wave will be focused by the concave part of the S-shape lens, but diffused by the convex part. Meanwhile, when the outgoing electromagnetic wave just crosses the upper interface of the S-shape lens, the simulation results of the average phase variation versus different frequencies [Fig. 5(c)] for S-shape lenses made of effective medium (blue dots) and realistic meta-atoms (black circle) indicate a near constant phase variation in the designed operating frequency range, implying the broadband ENZ response. And the mean value of the average phase variation is about 0.7 rad (red line) in the operating frequency range.

IV. CONCLUSIONS

In conclusion, based on the Bergman spectral representation of the effective permittivity, we have proposed a design to achieve the realistic broadband ENZ meta-atom consisting of steplike metal-dielectric multilayered stacks in optical frequency range. The broadband ENZ response is achieved due to the fact that the electric field can penetrate through the meta-atom through different paths corresponding to different ENZ frequencies. Functional optical devices with exotic electromagnetic properties, including directional emission and phase front shaping, over a wide frequency range of more than 50 THz have been constructed with the meta-atom, and these unconventional devices can find many applications in optical communications, imaging processing, energy redirecting, and adaptive optics. Furthermore, our design can also be used

TABLE II. Filling ratio of the gold inclusion and the thickness of each layer.

	f_i		d_i (nm)	
Layer	Theoretical	Approximated	Theoretical	Approximated
1	0.216392	0.22	43.6884	44
2	0.188523	0.19	19.2691	19
3	0.163955	0.16	37.0425	37

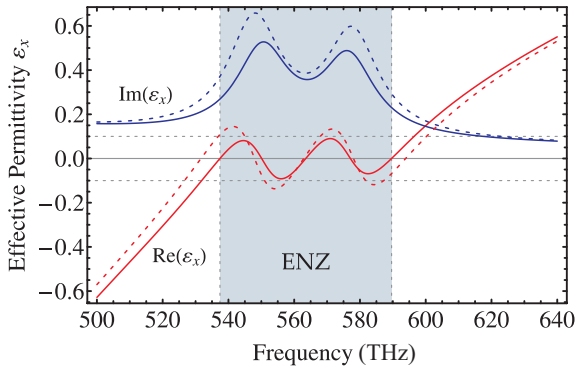

FIG. 6. (Color online) Robustness analysis of the designed parameters in the realistic meta-atom with solid curves indicating theoretical results in the main text based on six-digit values of the fraction and the thickness, while the dashed curves indicating the approximated results based on two-digit values.

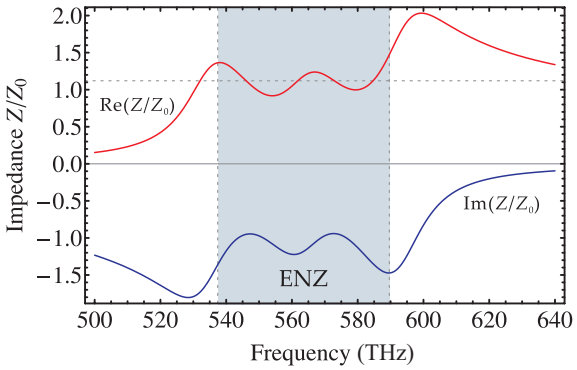

FIG. 7. (Color online) The impedance of the designed broadband ENZ metamaterials.

in designing metamaterials with other broadband constant parameters, such as magnetic permeability, electrical conductivity, and thermal conductivity and diffusivity.

ACKNOWLEDGMENTS

This work was partially supported by the Department of Mechanical and Aerospace Engineering, the Materials Research Center, the Intelligent Systems Center, and the Energy Research and Development Center at Missouri S&T, the University of Missouri Research Board, and the Ralph E. Powe Junior Faculty Enhancement Award.

APPENDIX

In order to achieve the best simulation results corresponding to the effective permittivity results depicted in Fig. 1 of the main text, the values of the gold inclusion filling ratio and the layer thickness for the realistic structures in Table I are calculated from the exact theoretical analysis and they are up to six significant digits mathematically.

In the practical fabrication, the feature size of the fabricated thin film has the accuracy of a nanometer. Regarding the robustness of the current design, a simple analysis is performed based on the theoretical design, with the results indicated in the above Table II and Fig. 6. As shown in Table II, the fraction and the thickness values are approximated into only two significant digits. According to Fig. 6, the effective permittivity calculated with the approximated two-digit values will only have a slight variation and small fluctuation, compared to the theoretical results obtained from the exact six-digit values in the manuscript. It is demonstrated that the performance of our design is quite robust to realistic fabrication tolerances.

On the other hand, the impedance marching with free space is of importance in practical applications. According to the obtained effective permittivity shown in Fig. 1(b), the impedance spectrum of the broadband ENZ metamaterial devices is plotted in Fig. 7. Within the broadband ENZ frequency region, the impedance also gives oscillatory response with the definition of $Z/Z_0 = \sqrt{\mu/\varepsilon_x}$, where Z_0 is the impedance of free space. Although the impedance is not perfectly matched with free space, the value is relatively low within the ENZ frequency region, which is a benefit from the existence of optical loss.

*To whom all correspondence should be addressed: yangxia@mst.edu

[1] V. G. Veselago, Sov. Phys. Usp. **10**, 509 (1968).
[2] J. B. Pendry, A. J. Holden, D. J. Robbins, and W. J. Stewart, IEEE Trans. Microw. Theory Tech. **47**, 2075 (1999).
[3] J. Valentine, S. Zhang, T. Zentgraf, E. Ulin-Avila, D. A. Genov, G. Bartal, and X. Zhang, Nature (London) **455**, 376 (2008).
[4] A. Alù and N. Engheta, Phys. Rev. E **72**, 016623 (2005).
[5] D. Rainwater, A. Kerkhoff, K. Melin, J. C. Soric, G. Moreno, and A. Alù, New J. Phys. **14**, 013054 (2012).
[6] J. B. Pendry, D. Schurig, and D. R. Smith, Science **312**, 1780 (2006).
[7] D. Schurig, J. J. Mock, B. J. Justice, S. A. Cummer, J. B. Pendry, A. F. Starr, and D. R. Smith, Science **314**, 977 (2006).
[8] Z. Liu, H. Lee, Y. Xiong, C. Sun, and X. Zhang, Science **315**, 1686 (2007).
[9] J. Shin, J. T. Shen, and S. Fan, Phys. Rev. Lett. **102**, 093903 (2009).
[10] M. Choi, S. H. Lee, Y. Kim, S. B. Kang, J. Shin, M. H. Kwak, K. Y. Kang, Y. H. Lee, N. Park, and B. Min, Nature (London) **470**, 369 (2011).
[11] X. Yang, J. Yao, J. Rho, X. Yin, and X. Zhang, Nat. Photonics **6**, 450 (2012).
[12] S. Enoch, G. Tayeb, P. Sabouroux, N. Guérin, and P. Vincent, Phys. Rev. Lett. **89**, 213902 (2002).
[13] M. Silveirinha and N. Engheta, Phys. Rev. Lett. **97**, 157403 (2006).
[14] M. G. Silveirinha and N. Engheta, Phys. Rev. B **76**, 245109 (2007).
[15] R. Liu, Q. Cheng, T. Hand, J. J. Mock, T. J. Cui, S. A. Cummer, and D. R. Smith, Phys. Rev. Lett. **100**, 023903 (2008).
[16] B. Edwards, A. Alù, M. E. Young, M. Silveirinha, and N. Engheta, Phys. Rev. Lett. **100**, 033903 (2008).
[17] A. Alù, M. G. Silveirinha, A. Salandrino, and N. Engheta, Phys. Rev. B **75**, 155410 (2007).

[18]S. Feng, Phys. Rev. Lett. **108**, 193904 (2012).
[19]Q. Cheng, W. X. Jiang, and T. J. Cui, Phys. Rev. Lett. **108**, 213903 (2012).
[20]M. G. Silveirinha, A. Alù, and N. Engheta, Phys. Rev. E **75**, 036603 (2007).
[21]A. Alù and N. Engheta, Opt. Express **15**, 3318 (2007).
[22]A. Alù and N. Engheta, Phys. Rev. Lett. **102**, 233901 (2009).
[23]A. Alù and N. Engheta, Phys. Rev. Lett. **105**, 263906 (2010).
[24]L. Sun and K. W. Yu, J. Opt. Soc. Am. B **29**, 984 (2012).
[25]D. J. Bergman, Phys. Rev. B **19**, 2359 (1979).
[26]D. J. Bergman and D. Stroud, Solid State Phys. **46**, 147 (1992).